LIGHT-INDUCED PARAMETRIC AMPLIFICATION IN MEMS OSCILLATORS

M. Zalalutdinov, A. Olkhovets, A. T. Zehnder, B. Ilic, D. Czaplewcki,
J.M. Parpia, H.G. Craighead

Cornell Center for Material Research, Cornell Univ., Ithaca NY14853

ABSTRACT

Micromechanical oscillators in the radio frequency (rf) range were fabricated in the form of silicon discs supported by a SiO_2 pillar at the disc center. Effective spring constant of this oscillator can be controlled within the range $\Delta f/f \sim 10^{-4}$ by a low power laser beam, ($P_{laser} \sim 100$ μW), focused at the periphery of the disc. Parametric amplification of the disc's vibrations was achieved through a double frequency modulation of the laser power. An amplitude gain of up to 30 was demonstrated, with further increase limited by non-linear behavior and self-generation. Phase dependence, inherent in degenerate parametric amplification, was also observed. Self-modulation of the CW laser beam ($P_{laser} \sim 100$ μW) provided by placing the disc oscillator into a interference pattern setup can lead to parametric self-excitation.

Keywords: MEMS, high-frequency, oscillator, parametric amplification, light pumping

1. INTRODUCTION

The smaller – the faster: scaling down the dimensions of microelectromechanical systems (MEMS) into the micron and submicron region shortens the response time down to nanoseconds. A bar clamped at both ends with dimensions 0.2x0.2x2 microns microfabricated from single-crystal silicon exhibits a resonant frequency of 380 MHz [1], extending the area of MEMS applications into the ultra-high frequency (UHF) region. UHF MEMS devices are expected to replace bulky and power-hungry elements in telecommunication devices, such as quartz oscillators, filters, frequency converters, etc. Since process of MEMS fabrication is compatible with modern silicon technology, micromechanical devices can be the basis for next generation UHF integrated circuits [2].

However, the way to transform an electrical signal into mechanical motion and vice versa represents one of the main challenges in MEMS applications. In the most straightforward filter configuration a MEMS oscillators would be driven electrostatically by an external voltage U_{ext} (signal from antenna), exhibiting mechanical vibrations when U_{ext} has a resonating frequency component. Such an UHV mechanical vibration with nanometer amplitude must be converted back into an electric signal for further processing. The high frequency of the mechanical motion practically excludes supersensitive but slow detection methods, such as electron tunneling, used in accelerometery [3] or magnetometry[4]. Capacitive method [5] and optical methods [1] are considered as the most suitable because of the fast response and high sensitivity. An optical method employing a focused laser beam allows a design not overloaded by closely placed electrodes, and also provides reduced cross-talk between driving and detection signals. Interferometric and beam-deflection techniques convert the intensity variation of the reflected laser beam (caused by mechanical motion) into electrical signal with subsequent amplification and measurement by an electric circuit. Being widely employed in force microscopy [6,7,8], optical detection technique was also used to achieve a force resolution of 5.6×10^{-18} N [9] and mass sensitivity of 10^{-12} g [10].

Laser wavelength puts a limit on the sensitivity of the interferometric method, making detection of nanometer motion problematic. Signal processing (amplification in this case) on the mechanical level, provided before the mechanic-to-electric conversion by an active UHF micromechanical components, can solve such a problem and is considered as a key point for future MEMS devices.

Parametric amplification represents a means for "mechanical signal processing" in regards to MEMS oscillators. The energy, necessary to gain mechanical motion is provided by periodic modulation of the oscillator's parameter – effective stiffness k [11]. Small mechanical vibrations, induced by a weak external force can be amplified by the parametric mechanism and the enhanced vibrations will be detected optically. Since a "mechanical parametric preamplifier" can be noise-free down to the quantum-mechanical level [12], it should greatly improve the signal-to-noise ratio of the resulting signal. A mechanical oscillator embedded in a degenerate parametric amplification scheme is also fundamentally interesting because mechanical squeezed states can be produced by such a system: the thermal vibration in one phase of the response can be reduced below the thermal equilibrium level [13]. In MEMS oscillators, the only method that has demonstrated parametric

Design, Test, Integration, and Packaging of MEMS/MOEMS 2001, Bernard Courtois, Jean Michel Karam,
Steven P. Levitan, Karen W. Markus, Andrew A. O. Tay, James A. Walker, Editors,
Proceedings of SPIE Vol. 4408 (2001) © 2001 SPIE · 0277-786X/01/$15.00

amplification is achieved by modulation of the effective spring constant by superimposing a time-varying electric field between the oscillator and an additional, closely located capacitor plate [13,14,15].

In this paper, we demonstrate a new method to establish mechanical parametric amplification in MEMS. In our system, a modulated intensity focused laser beam provides periodic (at double frequency) changes of the effective spring constant of the oscillator. The dc component of the laser beam is used to detect the vibration (at the fundamental frequency) by interferometric scheme. Optical pumping for parametric amplification does not require the oscillator to be conducting and does not need additional electrodes located in proximity to the oscillator. It can be easily integrated into existing, widely used optical detection techniques.

2. OSCILLATOR DESIGN

A high quality factor (Q) of the oscillator is necessary in order to minimize the amount of heat required to make the temperature-related effects noticeable. Careful design, avoiding points with high local stress concentration, minimizing clamping losses, could help to enhance the Q. Based on this consideration we have fabricated cylindrically-symmetric oscillators as discs supported by a single pillar at the center point. By minimizing the diameter of the supporting rod one should be able to reach the limit when such a structure is equivalent to a free disc. Commercially available silicon-on-insulator (SOI) wafers with a 250 nm thick silicon layer on top of a 1 micron silicon oxide layer were used for the microfabrication. Discs of radius R from 5 to 20 microns were defined by electron-beam lithography followed by a dry etch through the top silicon layer. Dipping the resulting structure into hydrofluoric acid undercuts the silicon oxide starting from the disc's periphery toward the center. By timing this wet etch, the diameter of the remaining column of the silicon oxide, which supports the released silicon disc, can be varied (Fig.1). In this paper we present data obtained with the R=20 microns discs supported by the SiO2 pillars with diameter 6.7 microns.

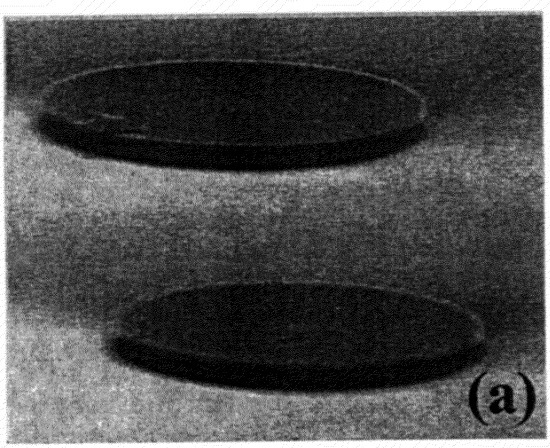

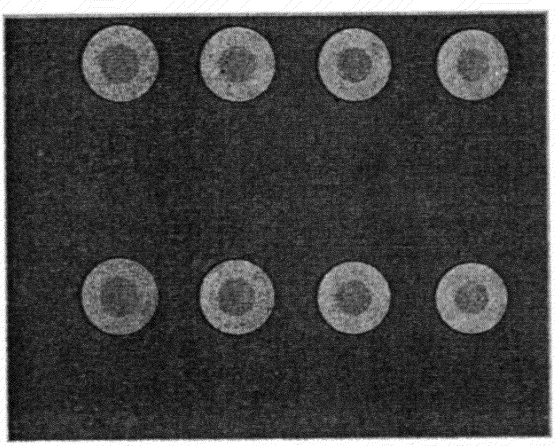

Fig.1 (a) Electron micrograph of the disc oscillators; (b) schematic view and (c) optical image.

After a critical point drying (CPD) process, samples were glued on a piezoceramic transducer and placed into a high vacuum chamber (P=10^-7 Torr). An AC voltage applied to a piezoceramic transducer, attached to the wafer, was used to excite the MEMS oscillators. These oscillations resulted in the variation of the gap between the disc and the silicon substrate and were detected by an interferometric technique with a He-Ne laser beam focused on the surface of the disc. All the measurements were done at room temperature.

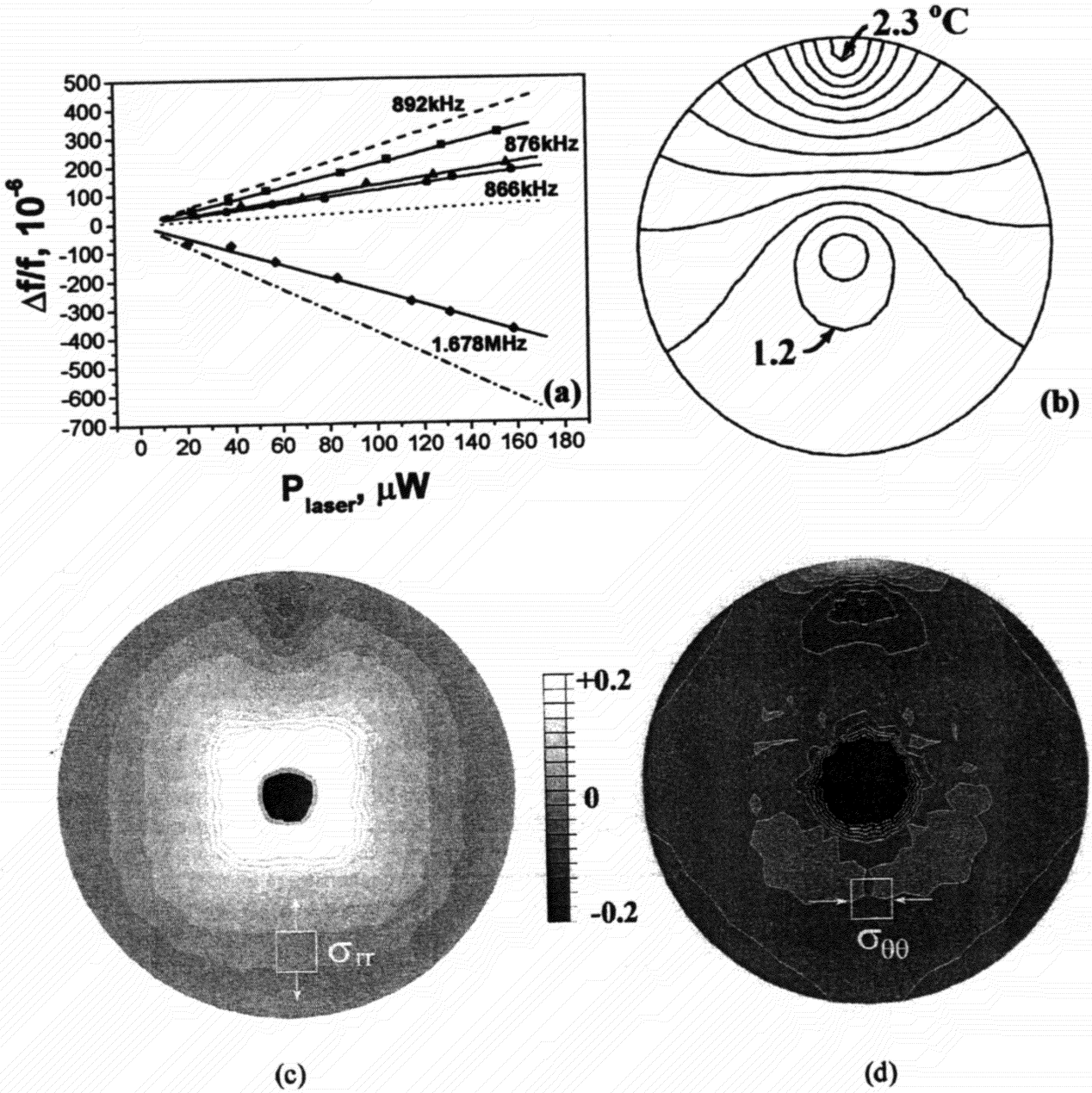

Figure 3, (a) Relative shift in frequencies versus incident DC laser power. Experimental data (circles correspond to 866kHz resonant peak, triangles - to 876 kHz, squares – to 892 kHz and diamonds – to 1.67MHz) are shown together with linear fits (solid lines). Dotted line, dash and dash-dot lines represent the results of the FEM calculations for the frequency shifts of the modes γ_{01}, γ_{00} and γ_{02} respectively. (b) Temperature field computed from finite element analysis. The model assumes 25% absorption of 260 μW DC laser power over a 5 micron diameter spot at edge of disk. Contour line spacing is 0.1C. (c,d) Two-dimensional stresses induced within the disc by the temperature distribution from Fig. 3b.

Analysis of the thermal stress induced within the disc by the focused laser beam provides the explanation of the observed resonant frequency behavior. For qualitative understanding, consider a simpler problem, a cylinder heated uniformly, with the inner diameter constrained, i.e. the displacement equals zero. (This models the constraint effect that the oxide pillar has on the Si disk.) One can solve this problem in two steps. First heat the cylinder and allow it to expand stress free. Then negative pressure should be applied to pull the inner diameter back to its starting dimension. This tension shifts the resonant frequency of the disc vibration.

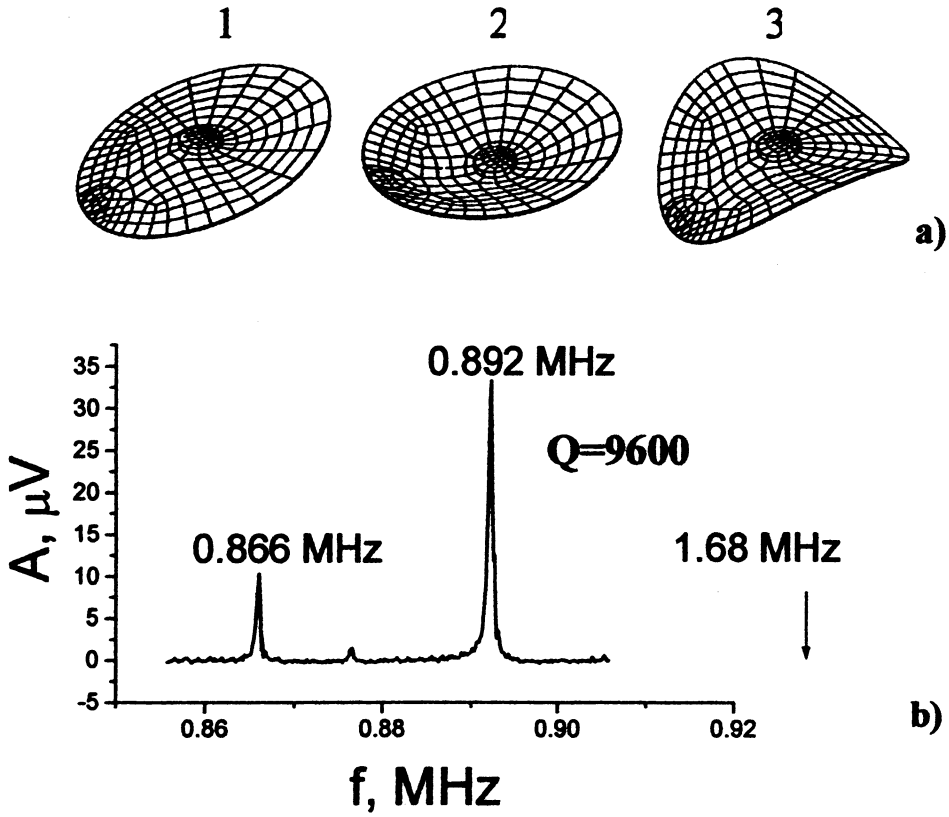

Fig.2 (a) Modes of the disc bending γ_{01} - (1), γ_{00} -(2) and γ_{02} -(3); (b) the corresponding resonant peaks of a disc (R=20μm, r=6.7μm) vibrations.

Plate vibrations are described by the fourth-order differential equation [16]:

$$\nabla^4\eta + \frac{3\rho(1-s^2)}{Eh^2}\frac{\partial^2\eta}{\partial t^2} = 0 \qquad (1)$$

where E is flexural modulus, s is Poisson's ratio, ρ is the density of the material and h is half-thickness of the plate [14]. Possible solution of the equation (1) are given by the expressions:

$$Y(r,\varphi) = \begin{matrix}\cos\\ \sin\end{matrix}(m\varphi)\left[AJ_m(\gamma r) + BI_m(\gamma r)\right] \qquad (2)$$

Coefficients A, B and γ_{mn} are defined by choosing boundary conditions (displacement and first derivative should be zeroed around the pillar while no bending or shearing forces exist on circumference of the disc). Figure 2a illustrated three modes of vibrations corresponding to γ_{10}, γ_{00} and γ_{20} marked as 1,2,3 respectively. For our structure (R=20μm, r=6.7μm), the highest quality factor 11,000 was observed for the mode γ_{00} of the disc oscillations with a frequency of 0.89 MHz. Results presented later in this paper are related to this particular resonance.

3. LIGHT-INDUCED STIFFNESS MODULATION

A low power laser beam (He-Ne, $P_{incident}$~100μW) focused on the periphery of the disc was found to be an effective tool to control the resonant frequency of the disc oscillator. Fig.3a demonstrates frequency shifts for all three modes shown on the vibration spectrum (Fig.2b) as a function of the incident laser power. Modes γ_{00} and γ_{10} demonstrate linear increase of the stiffness with the increased laser power, which is quite counterintuitive. At the same time, an expected decrease of the resonant frequency (i.e. softening) was observed for the high-frequency mode γ_{20}.

The scaling of frequency with temperature can be demonstrated by analogy with the problem of a pinned-pinned beam under thermal stress. In this case the frequency of the first mode of vibration [15] is

$$\omega = \omega_0 \sqrt{1 + \frac{12\sigma L^2}{Eh^2\pi^2}}$$

where ω_0 is the frequency when the thermal stress is zero, L is the length of the beam, and h is the thickness. The stress is given by $\sigma = -\alpha E \Delta T$, where α is the coefficient of thermal expansion, and ΔT is the temperature rise. Thus

$$\omega = \omega_0 \sqrt{1 - \frac{12\alpha \Delta T L^2}{h^2\pi^2}}$$

and the frequency shift due to heating of the beam is

$$\frac{1}{\omega}\frac{d\omega}{dT} = -\frac{6\alpha L^2}{\pi^2 h^2} \qquad (3)$$

We see from this model problem that the frequency should change linearly with temperature and that the shift is stronger for slender beams (L/h large). As an order of magnitude estimate of (1/ω)(dω/dT), taking L=10 μm, h=0.25 μm, α=2.5*10^{-6}/°C, yielding (1/ω)(dω/dT)=-0.002/°C.

Inhomogeneous temperature distribution across the disc makes the situation more complicated, requiring numerical methods, such as finite element (FEM) analysis. Using the FEM result that ΔT=1.25 °C across the disc for DC power of P_{laser}=260 μW, we arrive at a slope of 5.5*10^-4 /°C for mode 2 in Figure 3a, approximately one-fourth the magnitude of the shift in a beam. Note that in a disk there are two components (radial and hoop) of thermal stress within the disc and that they change in opposition to each other. So although for a beam one can only decrease frequencies by heating, one can both increase and decrease frequencies by heating the disk.

The frequencies, temperature and stress in the disk were computed using FEM analysis. The FEM solution modeled both the Si disk and the oxide base. We assumed that both the temperature and displacement were zero at the bottom of the oxide base. The model was meshed using 20 noded, three dimensional brick elements. Comparison of this model with a two dimensional shell model showed that both gave almost identical results, thus a simpler modeling approach can also be used. The computed temperature field for DC laser heating is shown in Fig.3b. For 260 μW power the maximum temperature rise is 2.35C. The temperature at the junction of the disk and pillar is 1.1°C, thus the temperature difference across the disk is ΔT=1.25°C. Due to thermal expansion, stresses develop in disk as shown in Figure 3c,d. In the radial direction the stresses, σ_{rr}, are primarily tensile, while in the hoop direction, $\sigma_{\theta\theta}$ is primarily compressive. The tensile radial stresses increase the frequency of modes with primarily radial bending. The compressive stresses decrease the frequency of modes with bending in the hoop direction. Good agreement between the results of FEM calculations and experimental data is demonstrated in Figure3a, where the modes γ_{01} and γ_{00} (shapes are shown in Fig.2a) increase in frequency with increasing laser power, while the frequency of the γ_{02} mode decreases with increasing laser power.

4. PARAMETRIC AMPLIFICATION

Modulation of the laser beam intensity can provide periodic change of the effective stiffness. Time-varying parameter causes mixing of two different modes of vibrations (in a same way as non-linear circuit provides mixing of two different modes of vibrations). That mixing allows energy supplied to the system at one frequency to be converted to another. For the case of degenerate parametric amplifier the modes to be coupled are two counter-rotating ones. Providing pumping frequency equal to the sum of the frequencies (which is a double frequency for the degenerate case) the pumping energy is fed into vibration at the fundamental frequency. Deriving the expression for the gain of a degenerate parametric amplifier we follow [11,13].

The equation of motion is:

$$m\frac{d^2x}{dt^2} + \frac{m\omega_0}{Q}\frac{dx}{dt} + \left[k_0 + k_p(t)\right]x = F(t) \qquad (4)$$

where x(t) is oscillator displacement, F(t) is an external driving force and ω_0 is the resonant frequency of the oscillator. It can be changed into two uncoupled differential equations through the use of normal-mode approach described by Louisell [11]. Transformation is introduced:

$$a = \frac{dx}{dt} + i\omega_1^* x; \qquad a^* = \frac{dx}{dt} - i\omega_1 x \qquad i = \sqrt{-1} \qquad \omega = \omega_0\left[\left(1 - \frac{1}{4Q^2}\right)^{1/2} + \frac{i}{2Q}\right]$$

The inverse transformations are:

$$x = \frac{a - a^*}{i(\omega_1^* + \omega_1)} \qquad \frac{dx}{dt} = \frac{\omega_1 a + \omega_1^* a}{\omega_1 + \omega_1^*}$$

Substituting them into the equation of motion (4) leads to a first-order differential equation:

$$\frac{da}{dt} = i\omega_1 a + i\frac{k_p(t)}{m}\frac{a - a^*}{\omega_1^* + \omega_1} + \frac{F(t)}{m}$$

If the driving force is applied in resonance $F(t) = F_0 \cos(\omega t + \varphi)$ and time-varied parameter k_p is oscillated at twice the resonant frequency $k_p = \Delta k \sin(2\omega_0 t)$, the last equation can yield the steady-state solution $a(t) = A\exp(i\omega t)$:

$$\left[i(\omega_1 - \omega_0)A - \frac{\Delta k}{2m(\omega_1^* + \omega_1)}A^* + \frac{F_0}{2m}e^{i\varphi}\right]e^{i\omega_0 t} = 0 \qquad (5)$$

For the oscillator with a high quality factor, Q, the relations $\omega_1^* + \omega_1 \approx 2\omega_0$ and $\omega_1 - \omega_0 \approx i\omega_0/2Q$ simplify equation (5):

$$A = F_0\frac{Q\omega_0}{k_0}\left[\frac{\cos(\varphi)}{1 + Q\Delta k/2k_0} + i\frac{\sin(\varphi)}{1 - Q\Delta k/2k_0}\right]$$

If the oscillator motion in the original system of coordinate can be described as $x(t) = X_1 \cos\omega_0 t + X_2 \sin\omega_0 t$, then $X_1 = \mathrm{Im}\,A/\omega_0$ and $X_2 = \mathrm{Re}\,A/\omega_0$. The total amplitude is therefore given by

$$X = \frac{F_0 Q}{k_0}\left[\frac{\cos^2\varphi}{1 + \frac{Q\Delta k}{2k_0}} + \frac{\sin^2\varphi}{1 - \frac{Q\Delta k}{2k_0}}\right]^{1/2} \qquad (6)$$

The high quality factor of the oscillator implies that small energy losses due to internal friction, clamping losses, etc. could be compensated by some low power external source of energy, leading to enhanced mechanical oscillations. Gain dependence on the phase shift φ between stiffness modulation $\Delta k(t)$ and driving force $F(t)$, following from the equation is also obvious from energetic consideration. In order to provide amplitude gain the increase of the stiffness Δk should occur around maximum of deflection, thus contributing to potential energy $E_p = (k + \Delta k)x^2$.

In our experiment, synchronization of the stiffness modulation with the motion of the oscillator was achieved by using the ac piezodrive voltage V_{piezo} as a reference signal. Schematic diagram of the experiment is shown in Fig.4. An external generator produces a double frequency ac voltage, phase locked with it. This voltage after amplification and phase shift is used to control the electro-optical modulator (EOM), which, by partial modulation, provides the double-frequency ac component of the intensity of the He-Ne laser beam focused on a < 5 micron spot on the surface of our disc oscillator.

With this parametric drive, a thirty times increase of the amplitude of the mechanical vibrations (Fig.4) was detected, when the ac component of the laser beam was increased to 100 microWatt (the power absorbed by the disc can be estimated as 10-15 microWatt). The corresponding width of the resonance peak becomes narrower by amplification, displaying an effective Q of up to 65 000. With a fixed amplitude of the optical pump (fixed gain of the parametric amplification) the system demonstrates linear mechanical response to the piezodriving voltage. The maximum observable gain is limited by the self-

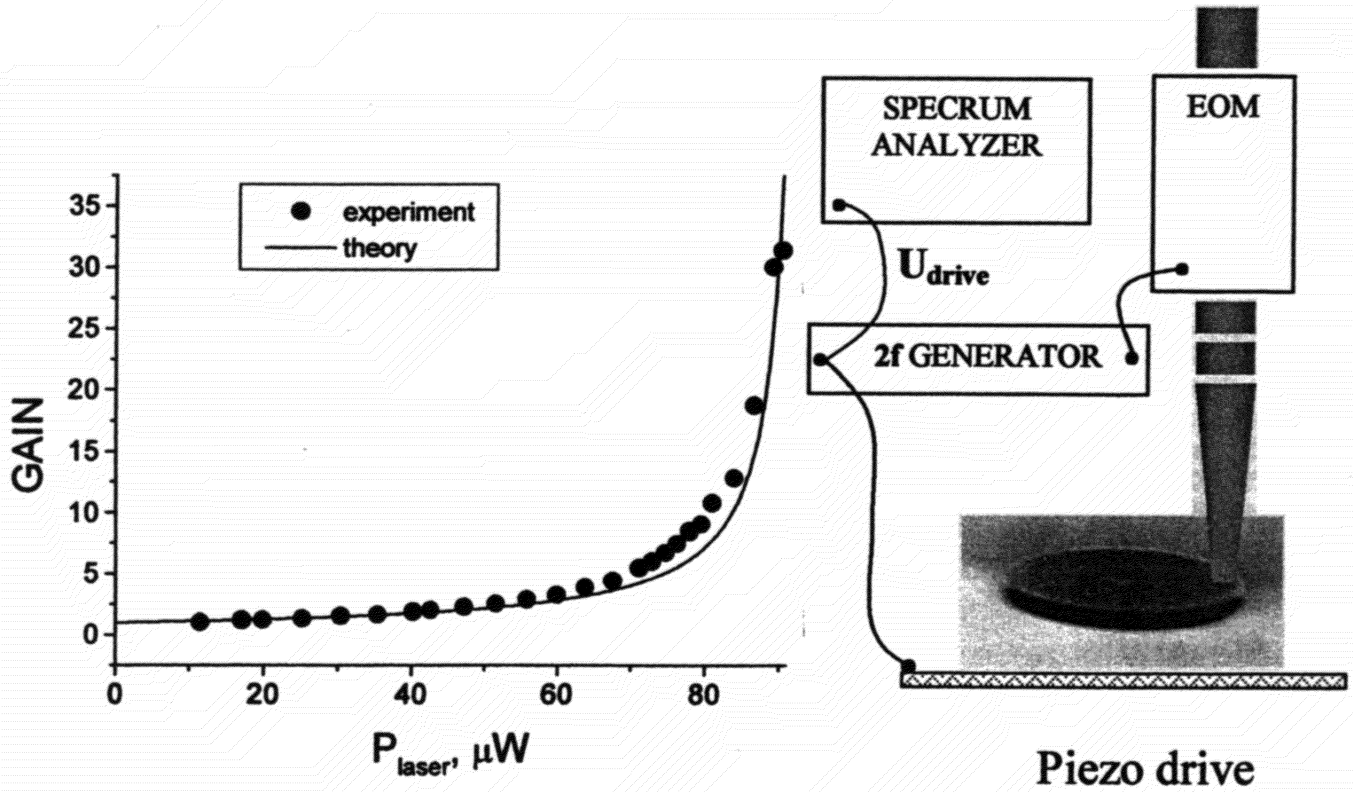

Figure 4 The parametric amplification gain versus amplitude of the laser power modulation. Experimental points are shown by black circles. The solid line is a fit according to equation (6). Schematic diagram of the experiment is shown on the right.

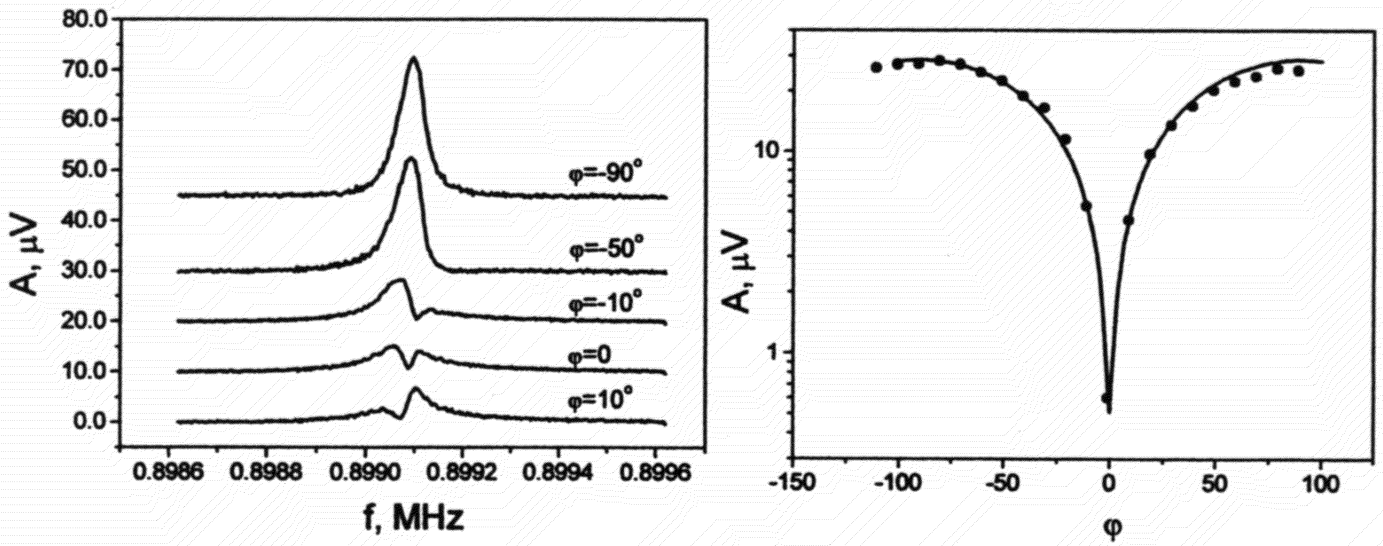

Fig.5 (a) Resonance curves obtained for different phase shifts φ of the optical pumping in respect to driving force. (b) Amplitude of the resonant peak as a function of the phase shift φ. Experimental results (black circles) are shown together with theoretical fit (solid line)

generation of the system. A critical parameter is the focus of the laser beam at the periphery of the disc to provide the best conditions for amplification.

The effect of the phase shift, φ, between the piezodrive and the optical pump is illustrated in fig.5a,b. The resonant response for φ=90° (maximum amplification) and φ=0 are shown in fig3b. The suppression of the vibrations at a phase φ=0 is clearly seen. The amplitude of oscillation as a function of the phase shift φ, shown in fig.5b was fitted by the theoretical expression that follows from equation (6). Excellent agreement between experimental data (black circles) and the theoretical prediction (solid line) was found.

Consistency between self-generation power threshold calculated from equation (6) for known $\Delta k(P_{laser})$ dependence (see Fig. 3a) and experimental data $P_{threshold}$~90μW (Fig.4) proves that heat absorption and thermal stress-induced stiffness modulation are the dominant mechanisms by which the laser beam interacts with the oscillator. Temperature-induced strain could be also accompanied by the stress created by photo-generated carriers [5,6]. This photo-induced stress in MEMS oscillator can be considered as another way to provide parametric amplification at high frequencies and low light intensity. By optimizing the laser wavelength and using a multilayer design for the oscillator one can significantly reduce the necessary laser power. These experiments are presently in progress.

5. SELF-GENERATION

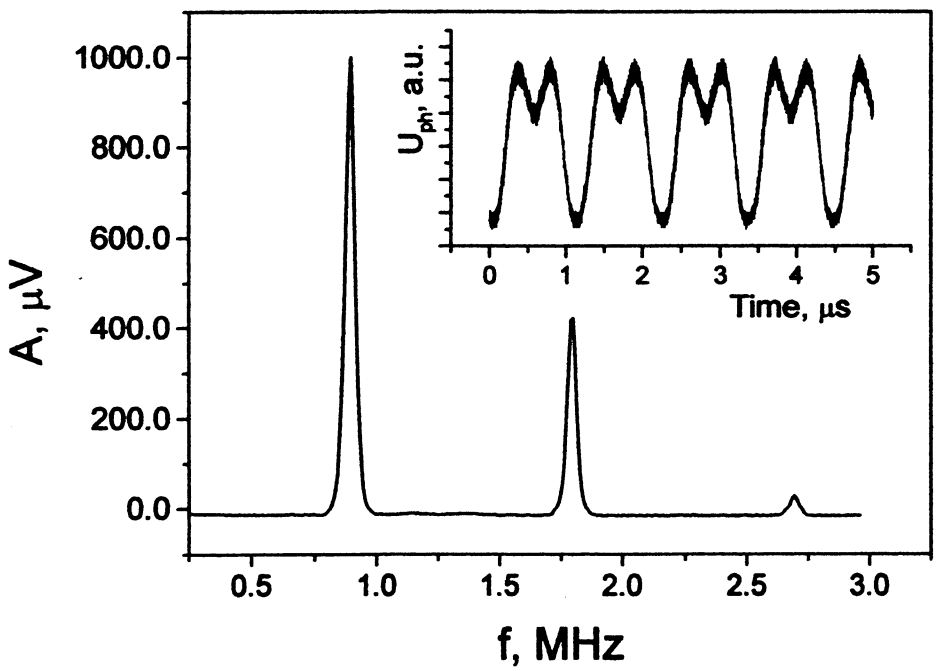

Fig.6 Spectrum of the disc oscillations excited by CW He-Ne laser beam P_{laser}=300μW. No piezodrive involved in experiment. Insert shows oscillogram of the signal from the photodetector.

Periodic modulation of the laser beam necessary to provide time-varying stiffness of the oscillator, was achieved by an external electro-optical modulator in the experiment described in section 4. However, the disc is part of an interferometric device, the gap between the disc and substrate affects the light intensity within the cross section of the disc (and hence – absorbed heating power) by changing interference conditions for reflected beams. Oscillation of the disc (initiated thermally for example) can cause modulation of the local disc heating even for CW laser beam. Non-linear dependence of the heating power versus gap value provides the presence of the second harmonic, necessary for parametric amplification. Phase shift between original mechanical vibrations and light modulation depends on the initial position of the disc within interferometric fringes. If starting conditions and laser beam intensity are chosen properly – self-amplification up to generation will occur.

Fig.6 shows spectrum of self-generated vibration stimulated by 300 μW CW laser beam (piezo drive is OFF). Generation is observed at the frequency corresponding to mode 2 in Fig.2. Dimples on the signal from photo detector (insert in Fig.6), which can also be seen as a strong second harmonic on vibration spectrum show that amplitude of oscillation is wide enough to hit next interferometric fringe.

To our best knowledge this is the first observation of parametric self-excitation in MEMS oscillators. Parametric mechanism makes our system different from optically-induced self-generation observed in bimorph MEMS oscillators [18,19]. Quality factor of a parametric generator and exact conditions for self generation are the subjects of our current research.

6. CONCLUSION

Parametric amplification with optical pumping was realized for radio frequency MEMS oscillator. A gain of 30 and effective quality factor Q=65,000 are demonstrated. Incorporation of parametric amplification into a signal processing for UHF MEMS devices is considered as a main goal. More generally, the parametrical amplification, described in this paper is a method to be used when small mechanical vibrations need to be detected. An enhanced quality factor and amplitude-phase dependence of a light-driven oscillator can be utilized for filtering, or when precise measurements of the frequency are necessary (for example, mass detection experiments). Parametric self-excitation of the MEMS oscillator by CW laser beam was demonstrated for the first time.

ACKNOWLEDGEMENTS

The authors are grateful to S. Turner for fruitful discussions. This work was supported by the Cornell Center for Materials Research (CCMR), a Materials Research Science and Engineering Center of the National Science Foundation (DMR-0079992).). Particular acknowledgment is made of the use of the Research Computing Facility of the CCMR.

1. D.W. Carr, S. Evoy, L. Sekaric, J.M. Parpia and H.G. Craighead Appl. Phys. Lett. 75, 920, (1999)
2. Clark T.C. Nguyen, Ark-Chew Wong, Hao Ding "Tunable, Switchable, High-Q VHF Microelectromechanical Bandpass Filters" IEEE Intl. Solid-State Circuits Conference, San Francisco, CA 448, 78 (1999).
3. D. Dilella, L.J. Whitman, R.J. Colton, T.W. Kenny, W.J. Kaiser, E.C. Vote, J.A. Podosek, and L.M. Miller, Sensors and Actuators A, A86, 8 (2000)
4. L. Cheng-Hsien, A.M. Barzilai, J.K. Reynolds, A. Partridge, T.W. Kenny, J.D. Grade, H.K. Rockstad, J.MEMS 7, pp235-44, (1998)
5. W.T. Hsu, J.R. Clark, C.T.-C. Nguyen "A Sub-Micron Capacitive Gap Process for Multiple-Metal-Electrode Lateral Micromechanical Resonators" IEEE Intl. Conference on Micro Electro Mechanical Systems MEMS 2001, Interlaken, Switzerland, January 21-25, 2001
6. Dror Sarid, Scanning Force Microscopy With Applications to Electric, Magnetic and Atomic Forces, New York Oxford University Press (1994).
7. J.A. Sidles, J.L. Garbini, K.J. Bruland, D. Rugar, O. Zuger, S. Hoen, and C.S. Yannoni, Rev. Mod. Phys. 67, 249 (1995).
8. M. Lohndorf, J. Moreland, P. Kabos, N. Rizzo J. Appl. Phys. 87, 5995 (2000)
9. T.D. Stowe, K. Yasamura, T.W. Kenny, D. Botkin, K. Wago and D. Rugar, Appl. Phys. Lett. 71, 288 (1997)
10. B. Ilic, D. Czaplewski, H. G. Craighead, P. Neuzil, C. Campagnolo, and C. Batt, Appl. Phys. Lett. 77, 451 (2000).
11. W.H Louisell "Coupled mode and parametric electronics" John Wiley & Sons, Inc. New York (1960)
12. C.M. Caves, Phys. Rev. D 26, 1817 (1982)
13. D. Rugar, P. Grutter Phys. Rev. Lett 67, 699 (2000)
14. D.W. Carr, S. Evoy, L. Sekaric, H.G. Craighead and J.M. Parpia, Appl. Phys. Lett. 77, 1545, (2000)
15. A. Olkhovets, D.W. Carr, J.M. Parpia and H.G. Craighead "Non-Degenerate Nanomechanical Parametric Amplifier" IEEE Intl. Conference on Micro Electro Mechanical Systems MEMS 2001, Interlaken, Switzerland, January 21-25, 2001
16. M. Morse "Vibration and sound" 2-nd edition, McGraw-Hill Book Company, Inc., New York, pp. 172-216, (1948)
17. P.S. Timoshenko, D.H. Young and W. Weaver, "Vibration Problems in Engineering", 4th edition, John Wiley and Sons, New York, pp. 453-455, (1974)
18. A.V. Churenkov Sensors and Actuators A, 39 pp141-148 (1993)
19. J.D. Zook, D.B. Burns, W.H. Herb, H. Guckel, J.W. Kang, Y. Ahn Sensors and Actuators A, 52 pp92-98 (1996)